WELDING RESEARCH

SUPPLEMENT TO THE WELDING JOURNAL, MAY 1975

Sponsored by the American Welding Society and the Welding Research Council

Analysis of Atmospheric Electron Beam Welding

A first step in the analysis of beams of higher power answers some questions but raises many others

BY J. H. FINK

ABSTRACT. This is a first step in the analysis of atmospheric electron beam welding for the purpose of understanding the process in order to make better weld setups and to design more effective machines. A theory is presented which shows the characteristic nail shaped weld cross-sections to be the result of surface and deep melting modes. The surface melting causes the nailhead configuration while the deep melting mode is responsible for the high ratio of weld penetration depth to width. In addition, studies are presented of melting efficiencies, which are compared to the results of 64 welding experiments.

Introduction

In order to promote general acceptance of atmospheric electron beam welding, it is essential that there be better understanding of the process. Specifically a theory is needed from which the required beam parameters, the allowable work speeds and work distances can be estimated to accomplish a particular weld design in any given metal.

With this in mind, an investigation was started, consisting of an analysis of some 64 welds run on different metals with various setups. It is to be expected that this is only a beginning of a long process of learning which will ultimately lead to better utilization of such machines and most probably to improved machine designs as well.

So far our success has been qualified. We have come to the seemingly obvious conclusion that control of the distribution of beam power density over the workpiece is vital in order to obtain repeatable results. Unfortunately, this is difficult to do as it depends upon two factors which are hard to evaluate, i.e., the initial distribution in the beam as it leaves the exit nozzle of the gun, and the subsequent scattering which occurs as the beam travels from the gun to the workpiece.

Although a detailed analysis of an electron beam traveling through and at the same time interacting with the air would present a formidable task, with the aid of some simplifying assumptions, we are able to present a crude mathematical model of the beam which seems to be applicable to the welding process as we know it. Unfortunately, we need more data to confirm our conclusions and to evaluate these relationships at both very high and very low welding speeds.

Welding Processes

The distinctive feature of electron or for that matter laser beam welds is their nail shaped cross-sections, with very large ratios of depth to width. While little is actually known about the process which forms such contours, it is assumed here, that they result from two different, but simultaneous, modes of melting.

As such beams cannot of themselves penetrate very far into solid or molten stock, the bulk of their energy must be carried into the interior of the solid workpiece by thermal conduction. Hence any subsequent melting occurs along an expanding perimeter whose ultimate contours, corresponding to the solution of what has been called (Ref. 1) a "Stephan problem", depend upon, among other things, the thermal properties of the workpiece, its size and temperature. This mode, which we call surface melting, is responsible for the characteristic shape of the "nail head".

Deep melting, on the other hand, relies upon the existence of a cavity in the workpiece directly under the beam, and the ultimate depth of penetration depends solely upon the limit of the ability of the beam to transport sufficient energy for melting to the bottom of the hole.

In some cases, more representative of cutting rather than welding, the molten metal is allowed to flow out of the melt zone. In other circumstances where the flow of the liquid metal is restricted, the beam creates a cavity that seemingly moves through the weld stock. Exactly how this occurs is not known; nevertheless, as the metal moves into the beam, it melts and flows around the beam to fill the weld cavity on the far side. Irrespective of the process, however,

J. H. FINK is Senior Engineer, Research and Development Center, Westinghouse Electric Corporation, Pittsburgh, PA 15235.

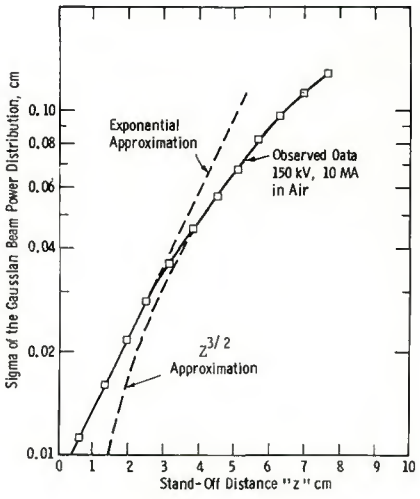

Fig. 1 — Comparing two approximations with observed values of the sigma of the Gaussian beam power distribution

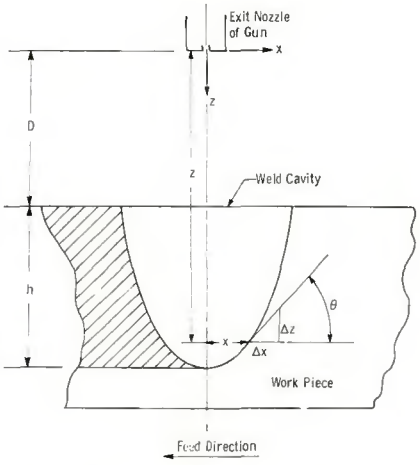

Fig. 2 — Schematic of weld cavity

the peak power density in the beam seems to be the critical parameter which establishes the maximum penetration depth.

Beam Power Density

According to multiple scattering theory (Ref. 2), an electron beam of zero cross-section entering a gas at z = 0, will spread into a power density distribution, at a distance z from the origin, that can be approximated by the following Gaussian function:

$$w(r) = \left(\frac{W_\sigma}{2\pi\sigma_z^2}\right) \exp\left\{\frac{-r^2}{2\sigma_z^2}\right\} \text{ W cm}^{-2}.$$

In this equation, W_σ represents the total beam power, r the radial coordinate of the beam, while σ_z, the sigma value of the distribution, is assumed to be:

$$\sigma_z^2 = \alpha Z^3 \quad \text{cm}^2 \qquad [1]$$

where α is given by:

$$\alpha = \left(\frac{2\pi}{3}\right) N \left(\frac{2Ze^2}{pv_e}\right)^2 \log_e \left(\frac{192\ p}{Z^{1/3}mc}\right)^{1/2} \text{ cm}^{-1}.$$

N represents the atomic density of the gas through which the beam travels, Z the weighted average of atomic numbers of the elements in the gas, e the electron charge, p the relativistic momentum of the electrons, m the electron mass, v_e the electron velocity and c the velocity of light.

Actually the beam cross-section is not Gaussian. In a recent theoretical study of beam broadening (Ref. 3) using Rutherford scattering and a Monte-Carlo scheme along with the established single scattering cross-sections, it was shown that the peak of the distribution can be roughly fitted to a Gaussian curve but the distribution at the extreme values of radius tend to be larger than the corresponding "wings" of the Gaussian curve.

As might be expected, most experimental studies have presented the beam power density distribution in any plane normal to the beam axis as very nearly Gaussian. However, there is some experimental data showing the sigma of that distribution to increase exponentially with the distance traveled by the beam (Ref. 4). From these observations, in contrast to Equation 1, it would seem that:

$$\sigma_z^2 = \sigma_o^2 \exp\left\{\alpha_j \rho_o z\right\} \quad \text{cm}^2 \qquad [2]$$

in which σ_o is the sigma at z = 0, ρ_o is the effective density of the gas through which the beam travels, and α_j is the beam attenuation constant, which can be approximated to within 15%, over the range of from 20 to 200 kV, by:

$$\alpha_j = \left(\frac{2.4 \times 10^{12}}{V^2}\right) \text{ cm}^2\ \text{g}^{-1}. \qquad [3]$$

The contradiction between Equation 1 and 2 was resolved to our satisfaction in an earlier set of experiments conducted with a rotating beam-profile analyzer on an electron beam traveling in air (Ref. 5). It was found that for large values of z, the results agree with Equation 1. However, for smaller z this equation is not applicable, as it is based upon the assumption of an initial electron beam of negligible cross-section. In the region of smaller z, the data shows reasonable agreement with Equation 2. These results are plotted in Fig. 1, where the transition from one relationship to the other occurs at about 3 cm from the exit nozzle of the gun.

We also learned from these experiments (Ref. 5) that, although the transverse beam power density could be approximated by a Gaussian curve, it actually had a peak value along the axis, which was higher than such a distribution would allow. Indeed with higher beam currents, the peak became disproportionally greater because of heating effects, which reduce the density of the gas in the path of the beam.

Despite this, we will approximate the beam power density distribution in the following analysis by:

$$w(r) = w(z) \exp\left\{\frac{-r^2}{2\sigma_z^2}\right\} \text{ W cm}^{-2}, \qquad [4]$$

in which w(z), the peak power density at z, is expressed as:

$$w(z) = \left\{\frac{W_o}{2\pi\sigma_z^2}\right\} \text{ W cm}^{-2} \qquad [5]$$

Deep Melting

If the work is fed along the x direction at a speed v, the portion of the beam striking the newly exposed metal must have sufficient power density to provide for its removal at a corresponding rate. Thus, if ρ is the metal density and H_m^* is the specific energy required for melting (including "warm-up" and heat of fusion), the absolute minimum power density required at any point on the front surface of the cavity must be:

$$w = \rho H_m^* v \qquad \text{W cm}^{-2} \qquad [6]$$

This assumes that the melting process is quasi-adiabatic, which is to say that the heat conduction losses are negligible because melting occurs during the thermal transient that exists before the heat has had a chance to be conducted away. Such a condition would never occur with flame or arc welding, as only electron beams or lasers can provide power densities of sufficient magnitude.

Assuming that at coordinate x from the beam axis and z from the exit nozzle (see Fig. 2) the cavity wall is at some angle θ to the horizontal, the power density coming from the beam will be distributed over an incremental surface such that, from Equations 4 and 5.

$$w = \left(\frac{W_o}{2\pi\sigma_z^2}\right) \exp\left\{\frac{-x^2}{2\sigma_z^2}\right\} \cos\theta \text{ W cm}^{-2} \qquad [7]$$

where σ_z is the sigma of the power density distribution in the cavity at coordinate z.

At the bottom of the cavity x equals zero and cos θ approaches one, therefore from Equations 6 and 7, we find the necessary maximum power density in the beam to be:

$$\rho H_m^* v = \left(\frac{W_o}{2\pi\sigma_h^2}\right) \text{ W cm}^{-2} \qquad [8]$$

in which σ_h corresponds to the sigma value of the beam power distribution

at the bottom of the cavity.

In the cavity it is assumed that the metal vapor density is such that the sigma value of the beam power distribution increases in a manner that is similar to Equation 2. Thus if σ_D is the sigma at the top of the workpiece;

$$\sigma_h^2 = \sigma_D^2 \exp\left\{(\bar{\alpha}_j\bar{\rho})h\right\} \text{ cm}^2, \quad [9]$$

in which $\bar{\alpha}_j$ is the attenuation constant of the beam in the vapor and $\bar{\rho}$ is the effective vapor density in the cavity. (Actually the "vapor" is a mixture of metal vapor, air, helium, or shielding gases in some unknown ratio, at some unspecified temperature; it is one of the significant undetermined values of our analysis).

From Equations 8 and 9 then, the penetration depth can be determined.

$$h = \left[\frac{1}{\bar{\alpha}_j\bar{\rho}}\right]\left[\log_e\left(\frac{W_o}{2\pi\sigma_D^2\rho H_m^* v}\right)\right] \text{ cm} \quad [10]$$

As the product $(\bar{\alpha}_j\bar{\rho})$ depends upon unknown vapor conditions in the cavity and σ_D^2 depends upon factors in the air above the workpiece, these terms are impossible to measure and can only be evaluated indirectly. This is accomplished in the following manner.

At a weld speed of one cm per second, let the corresponding penetration depth be designated as h_1; then:

$$h_1 = \left(\frac{1}{\bar{\alpha}_j\bar{\rho}}\right)\log_e\left(\frac{W_o}{2\pi\sigma_D^2\rho H_m^*}\right) \text{ cm.}$$

Similarly let the cut-off speed be designated as v_o under conditions that the penetration depth is zero, hence:

$$v_o = \left(\frac{W_o}{2\pi\sigma_D^2\rho H_m^*}\right) \text{ cm sec}^{-1}$$

By combining these equations we obtain:

$$\bar{\alpha}_j\bar{\rho} = (1/h_1)\log_e(v_o) \text{ cm}^{-1}$$

$$\sigma_D^2 = \left(\frac{W_o}{2\pi v_o \rho H_m^*}\right) \text{ cm}^2$$

It is assumed that σ_D^2 is a function of the distance D, from the exit nozzle of the gun to the surface of the workpiece, in accordance with either Equations 1 or 2, depending upon the magnitude of D.

LIST OF SYMBOLS

a	Fraction of beam power going into cavity
b	Deep weld width at half the penetration depth
b_m	Surface melt width
c	Velocity of light
C_o	Hablanian constant
C_s	Specific heat
D	Distance from exit nozzle of gun to the surface of the workpiece
e	Electron charge
f	Form factor when multiplied by product of weld width and weld depth results in weld area
f_1	Form factor for surface melt
f_2	Form factor for deep melt
h	Deep melt penetration depth
h_1	Deep melt penetration depth when weld speed equals one cm per second
h_m	Surface melt penetration depth
H_f	Heat of fusion
H_m^*	Specific energy of melting
m	Electron mass
N	Atomic density of gas through which the beam passes
p	Relativistic electron momentum
q_{cond}	Conduction losses from weld zone
r	Radial coordinate of the beam
T_D	Temperature difference between the melt temperature and the workpiece temperature prior to welding ($T_{melt} - T_{work}$)
T_m	Effective temperature ($T_D + H_f / C_s$)
T_{melt}	Melting temperature
T_{work}	Work piece temperature prior to welding
x	Beam coordinate in direction of welding
y	Beam coordinate perpendicular to welding
z	Beam coordinate into the work piece
Z	Weighted average of atomic numbers of the elements in the gas
v	Weld speed
v_e	Electron velocity
v_o	Cut-off weld speed when penetration depth is zero
V	Beam voltage
w(r)	Beam power density at radius r
w(z)	Beam power density along axis at a distance z from the exit nozzle of the gun
W_o	Total beam power
W_{in}	Beam power going into cavity
W_{melt}	Beam power which melts the work stock
W_{SM}	Beam power going into surface melting
α	Multiple scattering factor
α_j	Beam attenuation factor in air above weld
$\bar{\alpha}_j$	Beam attenuation factor in weld cavity
ε	Base of napierian logs
ρ	Workpiece density
$\bar{\rho}$	Effective gas density in weld cavity
ρ_o	Effective gas density above weld
λ_s	Thermal conductivity
λ_s^*	Thermal diffusivity
η	Melting efficiency
η_{DM}	Deep melting efficiency
η_{SM}	Surface melting efficiency
σ_D	Sigma value of beam power density distribution on the surface of the workpiece
σ_h	Sigma value at the bottom of the cavity
σ_z	Sigma value at any distance z
θ	Angle of weld cavity at coordinates x, y = 0, and z.

Surface Melting

As previously described the contours of surface melting are largely controlled by the size and condition of the workpiece, therefore it is impossible to specify a penetration depth for the general case. Nevertheless some idea of the significant factors of the weld setup, independent of the stock shape and temperature, can be obtained from the following approximations.

When a workpiece undergoes surface melting, the beam energy is deposited on the surface, from which it is subsequently conducted away. If it were assumed that all of the beam power entered the work at the spot where its surface intercepts the beam axis, these circumstances correspond to what Adams (Ref. 7) has called a three dimensional heat flow. Let the melt temperature equal the peak temperature located at a distance, equal to roughly half the melt width, from the weld path. Then the melt width, b_m, can be related to the weld speed and the total beam power, according to Adams, by the following formula:

$$T_D = \left(\frac{vW_o}{2\pi\lambda_s^*\lambda_s\varepsilon}\right)\left[\frac{1}{2+\left(\frac{vb_m}{4\lambda_s^*}\right)^2}\right] \text{ °C} \quad [11]$$

in which T_D is the difference between

the melting temperature and the temperature of the workpiece prior to welding, λ_s is the thermal conductivity and λ_s^* the thermal diffusivity of the weld stock, while W_o is the beam power going into the weld, v the weld speed and ϵ the base of napierian logarithms.

At reasonably high weld speeds;

$$(vb_m/4\lambda_s^*) > > 2$$

And in general:

$$\lambda_s/\lambda_s^* = \rho C_s \qquad [12]$$

where ρ is the density and C_s is the specific heat of the work. Therefore from Equation 11, the melt width can be approximated by:

$$b_m = \left[\frac{8\ W_o}{\pi\epsilon T_D \rho C_s v}\right]^{1/2} \text{ cm} \qquad [13]$$

Letting H_f represent the heat of fusion, T_{melt} the melting temperature and T_{work} the workpiece temperature prior to welding, an effective temperature, T_m, can be defined such that:

$$T_m = [T_{melt} - T_{work} + H_f/C_s] \ ^\circ C$$

Then if h_m represents the maximum depth of the molten bead, let f_1 be a constant such that $(h_m b_m f_1)$ equals the cross-sectional area of the weld zone. The melt efficiency of surface melting, defined as the ratio of power used for melting with respect to the total beam power, becomes:

$$\eta_{SM} = \frac{(b_m h_m f_1) v T_m \rho C_s}{W_o} \qquad [14]$$

Combining Equations 13 and 14, the penetration depth is found to be:

$$h_m = \left(\frac{W_o}{v}\right)^{1/2} \left(\frac{\pi\epsilon T_D}{8\rho C_s}\right)^{1/2} \left(\frac{\eta_{SM}}{f_1 T_m}\right) \text{ cm.} \qquad [15]$$

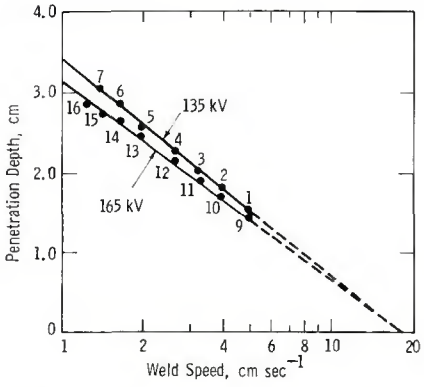

Fig. 3 — Weld data comparison of 36.5 kW, 135 kV and 36.6 kW 165 kV welding of 304 SS with a 0.95 cm standoff

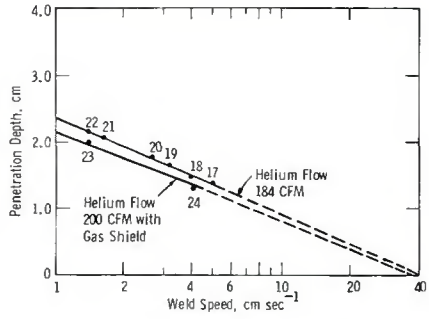

Fig. 4 — Weld data comparison of helium flow during 39.3 kW, 165 kV welding of copper with a 0.95 cm standoff

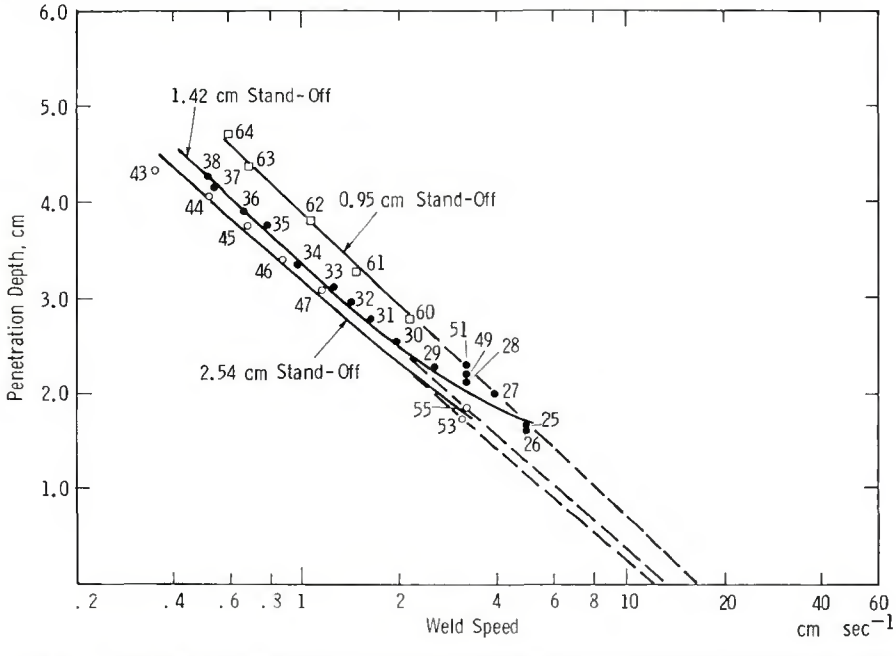

Fig. 5 — Weld data comparison of various standoff distances on 1020 hot rolled steel welds at 52.8 kW, 165 kV

Analysis of Welding Experiments

As stated earlier, a series of 64 welds were made with several metals under various conditions. The results, consisting of curves showing the penetration depth as a function of the log of weld speed are presented in Figs. 3, 4 and 5, along with tabulated data in Table 1. It is most significant that each set of data tends to follow a straight line. Despite the gross assumptions, the general form of Equation 10 agrees with the observed data reasonably well.

However, there are some anomalies that require explanation. Figure 3, for instance, presents a comparison of welds done on 304 stainless steel at 36.5 kW and 135 kV with those done at 36.6 kW and 165 kV. Surprisingly the lower voltage beam caused the greater penetration.

With reference to Table 1, it can be seen that the calculated values of σ_D^2 indicate that at the surface of the workpiece both beams were similar despite the voltage difference. However, the calculated value of $(\overline{\alpha}_j \overline{\rho})$ for the higher voltage beam is greater than the value obtained for the lower despite Equation 3 which indicates that the attenuation constant $\overline{\alpha}_j$ should be inversely proportional to the square of the beam voltage. To account for this discrepancy, the effective gas density in the cavity for the high voltage beam must have been greater by almost 165%!

Although at the lower voltage more energy is absorbed by the gas, leading possibly to a higher temperature, such a variation in density is an unlikely consequence of a change in beam voltage. Subsequent tests will have to be made to evaluate this effect. On the other hand there is evidence to show that the flow of protective gas, helium, can make a marked difference in the quantity $(\overline{\alpha}_j \overline{\rho})$. Therefore the seeming discrepancy may have actually resulted from an undetected difference in the flow of protective gas.

Figure 4 shows data taken from welds made on copper at 39.3 kW and 165 kV. Here two curves are shown which represent a difference in the gas flow which was deliberately introduced. With a change in flow from 184 to 200 CFM, the calculated value of $(\overline{\alpha}_j \overline{\rho})$ changed from 1.55 to 1.70 cm^{-1}. Meanwhile, the overall change in the values of $(\overline{\alpha}_j \overline{\rho})$ calculated for welds in 304 stainless steel as compared to those in copper can be attributed to the difference in beam attenuation resulting from differences in their respective metal vapors.

A comparison of welds made on 1020 hot rolled steel at different standoff distances is shown in Fig. 5. The curves observed in the data are dis-

cussed subsequently.

Referring to Table 1, the values of $(\overline{\alpha_j}\,\overline{\rho})$ are found to be relatively independent of the standoff distance. On the other hand the values of σ_D^2 vary with D in such a manner that it is evident that Equation 1 is not applicable. Therefore the sigma at the bottom of the cavity, σ_h, can be described in accordance with Equations 2 and 9, i.e.:

$$\sigma_h^2 = \sigma_o^2 \exp\left\{(\overline{\alpha_j}\,\overline{\rho})h + (\alpha_j\rho)D\right\} \text{ cm}^2.$$

And from Equation 8:

$$(\overline{\alpha_j}\,\overline{\rho})h + (\alpha_j\rho)D = \log_e\left(\frac{W_o}{2\pi\sigma_o^2 v\rho H_m^*}\right)$$

As a result, with a given beam power, voltage and weld speed, the sum of $(\overline{\alpha_j}\,\overline{\rho})$h plus $(\overline{\alpha_j}\,\overline{\rho})$D should be a constant. Unfortunately, there is insufficient data to demonstrate this relationship.

Additional weld data was obtained from experiments conducted at the Westinghouse, Sykesville, Maryland plant (Refs. 8, 9). As shown in Figs. 6 and 7, the tendency for linearity between the penetration depth and the log of the weld speed is very evident. However, at higher speeds the weld depth is greater than might be expected. Thus it appears that as the deep melting becomes shallower, the surface melting becomes dominant. This phenomenon is illustrated in Fig. 8, a replot of some of the data in Fig. 7. Here we see at high weld speeds (towards the left of the graph in Figure 8) the penetration depth is a simple function of the ratio of beam power to weld speed, as might be expected from Equation 15.

Melting Efficiency

For deep melting, the penetration depth, h, was shown to be a function of the peak energy density available from the impinging beam. Unfortunately, the weld width cannot be so easily specified because it is established ultimately by a process that is identical with surface melting, resulting from the distribution of beam energy over the cavity walls. Nevertheless some idea of the cross-sectional area of the deep melt zone can be obtained purely from considerations of beam power utilization, which can be determined from an inspection of the weld.

Neglecting radiation and convection, the power going into the weld equals that used for melting plus that carried away by conduction into the moving stock and that lost by evaporation of metal out of the cavity.

Designating b as the melt width at half the penetration of the deep weld, see Fig. 9, and f_2 as a form factor such

Table 1 — Weld Data From Figures 3, 4 and 5

Test nos.	Material	Weld power kW	Weld voltage kV	Standoff dist., cm	Penetration depth, h_1 cm	Cut-off speed, v_o cm/s	$\overline{\alpha_j}\,\overline{\rho_o}$ cm^{-2}	σ_D^2 cm^2	Fig
1-7	304 SS	36.5	135	0.95	3.45	18.0	0.84	.035	3
9-16	304 SS	36.6	165	0.95	3.12	18.0	0.93	.035	3
17-22	Copper	39.3	165	0.95	2.38	40.0	1.55	.026	4
23,24	Copper	39.3	165	0.95	2.15	39.0	1.70	.026	4
60-64	1020 HRS	52.8	165	0.95	3.87	17.0	0.73	.049	5
25-40 49.51	1020 HRS	52.8	165	1.42	3.35	13.0	0.72	.064	5
43-47 53,55	1020 HRS	52.8	165	2.54	3.20	12.0	0.77	.070	5

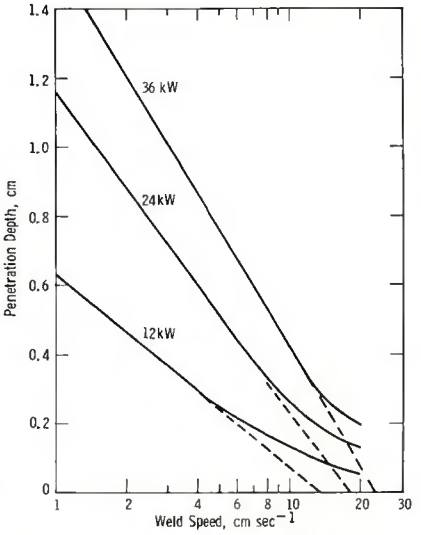

Fig. 6 — Weld data comparison of various beam powers, 1010 cold rolled steel, standoff: 0.97 cm (Ref. 8)

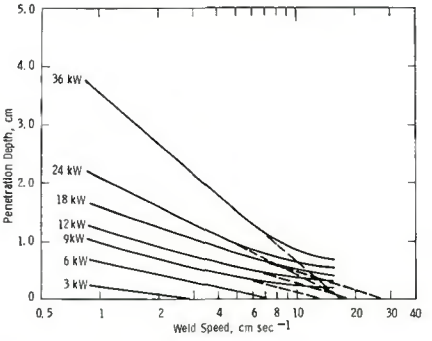

Fig. 7 — Weld data comparison of various beam powers, 1010 cold rolled steel, standoff: 0.97 cm (Ref. 8)

that (hbf_2) equals the cross-sectional area of the deep weld, the power used for melting can be described as:

$$W_{melt} = (hbf_2)vT_m\rho C_s \text{ W.} \qquad [16]$$

As the deep weld results from the presence of a cavity, the conduction losses to the workpiece can be approximated by assuming that they take place uniformly along the axis of the beam, moving at velocity v through a workpiece whose thickness equals the weld penetration depth, h. This is the same as the line source case described by Adams (Ref. 7), where the melting temperature corresponds to the peak temperature at a distance from the source path equal to roughly one half the melt width. Under these circumstances, and for the case of higher weld speeds, where,

$$(vb/4\lambda_s^*) >> 2 \qquad [17]$$

the conduction losses can be approximated by:

$$q_{cond} = \left(\frac{\pi\varepsilon}{2}\right)^{1/2} T_D\rho C_s vbh \text{ W.}$$

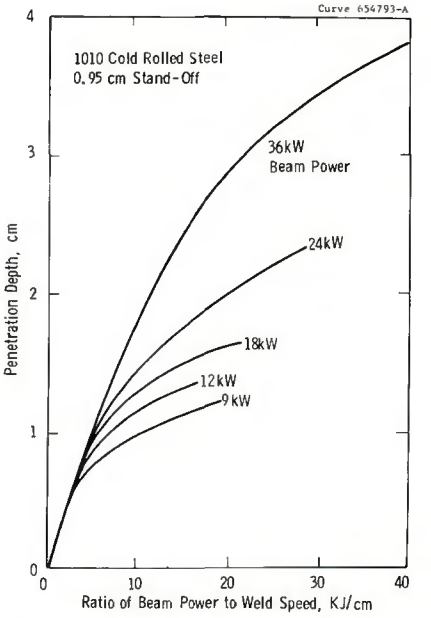

Fig. 8 — Energy expended per unit weld length (Ref. 8)

Although the power lost to evaporation out of the vapor cavity may be significant in vacuum welding where nothing hinders the vapor movement, it is only important in atmospheric welding at low speeds with high power beams, where the vapor cavity is large. At the more

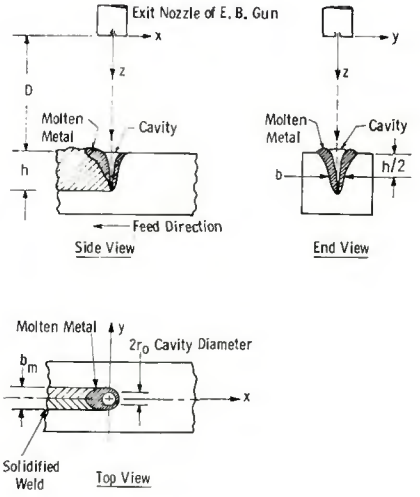

Fig. 9 — Atmospheric EB deep weld cross-sections (Ref. 17)

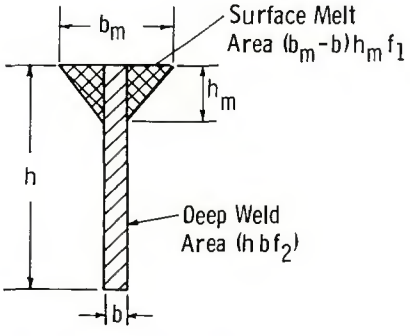

Fig. 10 — EB weld cross-section

common weld speeds and powers, it can be ignored. Hence, the power balance in a deep weld can be described by:

$$W_{in} = W_{melt} + q_{cond} \quad W,$$

or from Equations 16 and 17:

$$aW_o = (hbf_2)\, vT_m\rho C_s + \left(\frac{\pi\epsilon}{2}\right)^{1/2} T_D\rho C_s vbh \quad W \qquad [18]$$

in which 'a' represents that fraction of the total beam power which goes into the cavity.

If we define the melting efficiency as the ratio of the power required for melting to the total beam power, then for deep welding it can be evaluated from Equation 18 as:

$$\eta_{DM} = \left[\frac{a}{1 + \left(\frac{\pi\epsilon}{2}\right)^{1/2}\left(\frac{1}{f_2}\right)\left(\frac{T_D}{T_m}\right)}\right] \qquad [19]$$

When an electron beam has sufficient power density to cause deep melting, a certain portion of the power in the beam spills over onto the work surface causing a region of surface melting to surround the deep weld. The resulting weld cross-section can

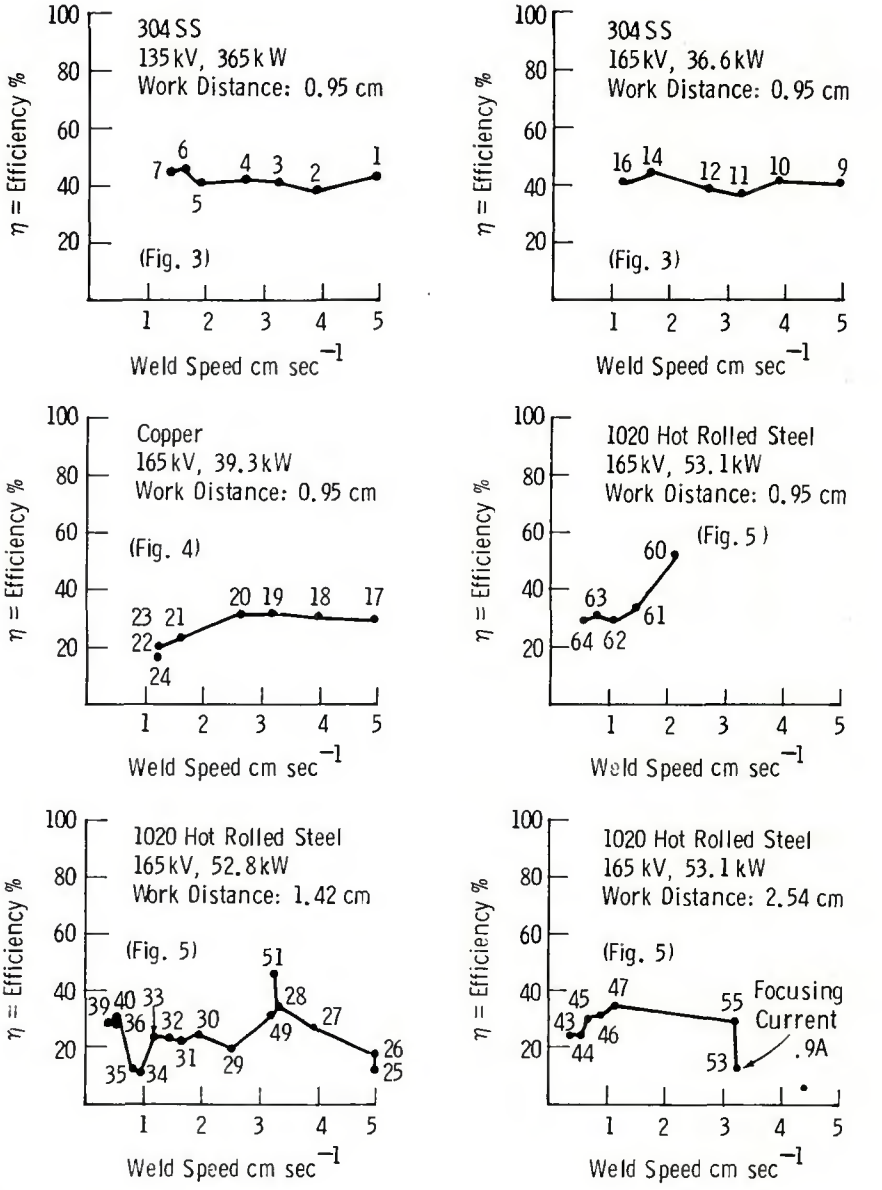

Fig. 11 — Melting efficiencies

be approximated as shown in Fig. 10.

In this case the power used for surface melting is:

$$W_{SM} = f_1 h_m (b_m - b)\, vT_m\rho C_s \quad W$$

in which the product $f_1 h_m(b_m - b)$ represents the cross-sectional area of the surface melt.

The conduction losses meanwhile can be approximated by means of equation 11, so that:

$$q_{cond} = \left(\frac{\pi\epsilon}{8}\right) T_D\rho C_s v(b_m - b)^2 \quad W.$$

The power balance equation for surface melting in the presence of deep welding is then:

$$W_o(1 - a) = f_1 h_m (b_m - b) vT_m\rho C_s + \left(\frac{\pi\epsilon}{8}\right) T_D\rho C_s v(b_m - b)^2 \quad W$$

in which $W_o(1 - a)$ represents that fraction of the total beam power that does not go into the cavity.

Hence, the surface melting efficiency is:

$$\eta_{SM} = \left[\frac{(1 - a)}{1 + \left(\frac{\pi\epsilon}{8}\right)\left(\frac{1}{f_1}\right)\left(\frac{T_D}{T_m}\right)\left(\frac{b_m - b}{h_m}\right)}\right]. \qquad [20]$$

The total melting efficiency η, meanwhile, is the sum of the deep weld and the surface melting efficiencies. Hence:

$$\eta = \eta_{SM} + \eta_{DW}$$

And from Equations 19 and 20:

$$\eta = \frac{a}{1 + \left(\frac{\pi\epsilon}{2}\right)^{1/2}\left(\frac{1}{f_2}\right)\left(\frac{T_D}{T_m}\right)} + \frac{(1 - a)}{1 + \left(\frac{\pi\epsilon}{8}\right)\left(\frac{1}{f_1}\right)\left(\frac{T_D}{T_m}\right)\left(\frac{b_m - b}{h_m}\right)} \qquad [21]$$

Various properties of metals are listed in Table 2 from which it can be seen that the ratio T_D/T_m is approximately 0.66 for those metals listed. Meanwhile, in most welds, f_2 is about one and f_1 one-half. As a result, assuming that $(b_m b)/h$ equals one, the denominators in both terms of Equation 21 are of the same approximate value. Hence the melting efficiency becomes relatively independent of the weld speed, and turns out to be about 40%.

The melting efficiencies of all of the experiments conducted in this work are plotted in Fig. 11. As displayed, it would appear that 40% is a reasonable estimate of the melt efficiency although some of the data is so erratic that it is difficult to draw a general conclusion. Actually, however, the irregularity of these results can be attributed more to the difficulty of making precise weld area measurements at one or two random cross-sections, than to nonuniformities in the melting process itself.

Neverthless, it should be recognized that the melting efficiency equation presented here is a crude approximation at best, which can only be hoped to be reasonably accurate in a limited range of weld speeds.

At high speeds approaching cut-off the deep melting process becomes shallower than that of the surface melting. Hence all of the energy going into the deep weld actually contributes to surface melting, causing the factor 'a' to equal zero. As a result, the welding efficiency in Equation 15 approaches a constant value of about 40% and the penetration depth becomes proportional to the square root of the ratio of beam power to weld speed.

Meanwhile at low speeds, the aforementioned relationships are invalid because the equations adapted from Adams' work are not applicable. Actually very little is known about low speed, high power welding.

Graphical Presentations of Weld Data

In the literature several types of graphs are used to display typical weld data. In this section we shall discuss two such plots and their significance with respect to atmospheric electron beam welding.

A common presentation of weld data (Refs. 10-15) displays the penetration depth h plotted against the expended energy per unit area, taken in the direction of the weld, i.e., (W_o/hv). From Equation 14 we find:

$$\left[\frac{W_o}{h_m v}\right] = b_m (f_1/\eta_{SM})\ T_m \rho C_s \quad Jcm^{-2}$$

Therefore at higher weld speeds where most of the beam power goes into surface melting and (f_1/η_{sm}) is constant, a plot of W /(hv) versus h presents some idea of the variation of the melt width, b_m, as a function of the penetration depth, h. However, at lower speeds, the ratio of the form factor, f_1 to the surface melting efficiency is no longer constant and, as a result, this type of plot loses its significance.

Table 2 — Various Properties of Metals (Ref. 6)

Property	Symbol	304 S.S.	Copper	1020 HRS	Units
Density	ρ	8.0	8.9	7.8	g/cm³
Heat of fusion	H_f	300	205	270	J/9
Specific heat	C_s	0.50	0.38	0.45	J/g-C
Working temperature	T_W	100	100	100	C
Melting temperature	T_M	1427	1083	1516	C
$(T_M - T_W)$	T_D	1327	983	1416	C
	(H_f/C_s)	600	540	600	C
$(T_M - T_W + H_f/C_s)$	T_m	1927	1523	2016	C
	T_D/T_m	0.69	0.64	0.70	
Thermal conductivity	λ_s	0.15	3.88	0.53	W/cm-C
Thermal diffusivity	λ_s^*	0.037	1.14	0.15	cm²/s
Specific Energy of melting	H_m^*	1170	685	1300	J/g

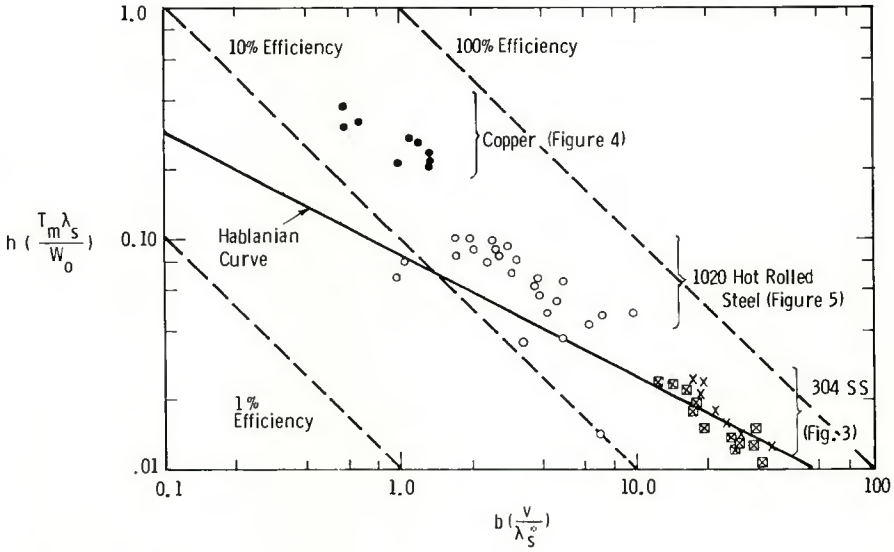

Fig. 12 — Hablanian plot

An important graphical presentation for vacuum electron beam welding was devised by Hablanian (Ref. 16) utilizing the dimensionless coordinates $(hT_m\lambda_s/W_o)$ and (bv/λ_s^*). He showed that most vacuum welds tend to follow the following empirical relationship:

$$\left[\frac{hT_m\lambda_s}{W_o}\right] = C_o \left[\frac{\lambda_s^*}{bv}\right]^{1/2} \qquad [22]$$

in which C_o was a constant (approximately equal to 0.09).

The significance of the Hablanian plot can be appreciated by considering a general expression for welding efficiency:

$$\eta = \frac{hbf\ v\ T_m \rho C_s}{W_o}$$

From Equation 12, this can be expanded into:

$$\left[\frac{hT_m\lambda_s}{W_o}\right] = (\eta/f)\ \frac{\lambda_s^*}{bv} \qquad [23]$$

Therefore, assuming that f = 1 as in the case of deep welds, lines of constant efficiency can be added to the Hablanian plot. This is done in Fig. 12 where all of the data from this series of experiments is displayed.

By combining Equations 22 and 23, it can be shown that the vacuum melting efficiency described by Hablanian must be of the form:

$$\eta = f\ C_o \left[\frac{bv}{\lambda_s^*}\right]^{1/2}$$

This is shown in Fig. 12 as the Hablanian curve (experimental data points not given) and it shows a marked difference between low power vacuum welding and high power atmospheric welding, (data points only).

(Continued on page 152-s)